THE JOURNAL OF PHYSICAL CHEMISTRY C
A JOURNAL OF THE AMERICAN CHEMICAL SOCIETY

pubs.acs.org/JPCC

Article

Surface Normal Lasing from CdSe Nanoplatelets Coupled to Aluminum Plasmonic Nanoparticle Lattices

Published as part of The Journal of Physical Chemistry virtual special issue "125 Years of The Journal of Physical Chemistry".

Nicolas E. Watkins, Jun Guan, Benjamin T. Diroll, Kali R. Williams, Richard D. Schaller, and Teri W. Odom*

Cite This: *J. Phys. Chem. C* 2021, 125, 19874−19879

Read Online

ACCESS | Metrics & More | Article Recommendations | Supporting Information

ABSTRACT: This paper describes low-threshold lasing from colloidal CdSe nanoplatelets (NPLs) coated on two-dimensional plasmonic cavities composed of aluminum nanoparticles (NPs). We designed the NP lattice to support a spectrally narrow surface lattice resonance whose wavelength overlapped with the amplified spontaneous emission (ASE) from CdSe NPLs. Al NP lattices coated with CdSe NPL thin films were optically pumped and exhibited lasing in the surface normal direction with low angular divergence, narrow spectral line width (∼1 nm), and a threshold of ∼200 $\mu J/cm^2$. Nonlinear light emission characteristics were found to depend on the thickness of the CdSe NPL film. A minimum thickness of 150 nm was required to observe SLR-mediated lasing, but thinner films exhibited only photoluminescence. Films above 150 nm exhibited both in-plane waveguided ASE from the CdSe NPL film and lasing action from the Al NP lattice.

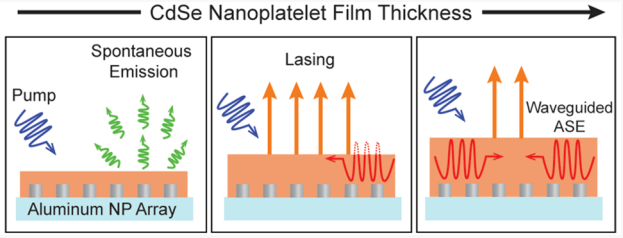

INTRODUCTION

Semiconductor nanoplatelets (NPLs) are promising for optoelectronic technologies such as light-emitting diodes and compact lasers due to their scalable synthesis, facile solution processing, narrow band-edge emission spectra, and large optical gain coefficients.[1−8] Similar to 2D quantum wells, NPLs can be synthesized with an identical number of vertically defined monolayers and have comparatively large lateral dimensions for tunable, homogeneously broadened band-edge absorption and photoluminescence.[2] NPLs also offer advantages for gain and lasing relative to zero-dimensional quantum dots:[9,10] the narrow band-edge line widths aid light amplification, the large lateral sizes (25 nm length × 4 nm width × 1.5 nm thickness) boost absorption cross sections by an order of magnitude,[11] and multiexciton lifetimes needed for population inversion can exceed those of the smaller-volume quantum dots from slower rates of Auger recombination.[12−16] However, optical gain lifetimes for single-component (core-only) NPLs are subnanoseconds, and small cavity sizes are needed for light amplification.

Lasing action requires a cavity that provides low-loss constructive optical feedback at one or more wavelengths within the supported spectral profile of a population-inverted gain medium.[17] Light amplification using semiconductor nanostructures has been demonstrated by using a wide variety of compact cavity architectures including whispering gallery mode resonators,[18,19] distributed feedback gratings,[20,21] vertical cavities,[15,22] and photonic crystals.[6,23] We have reported how 2D plasmonic nanoparticle (NP) lattices can act as nanolaser cavities for colloidal quantum dots,[24,25] upconverting nanoparticles[26] as well as organic dyes.[27−34] Plasmonic NP lattices support two types of plasmons: (1) localized surface plasmons (LSPs), arising from collective electron oscillations in isolated metal NPs, and (2) surface lattice resonances (SLRs), which are LSPs coupled to Bragg modes defined by lattice periodicity.[35−37] Several design parameters influence SLR characteristics such as lattice symmetry and spacing,[38−40] refractive index of the substrate, medium surrounding NPs, NP size, and materials composition.[41−47] When NP lattices are of high quality, the SLRs exhibit remarkably narrow spectral features (a few nanometers)[43,48] that influence laser characteristics including spectral width,[31,33] directionality of emission,[25,32,49] temporal profile,[50,51] and polarization.[24]

Here we report the lasing characteristics of CdSe NPL films on Al NP lattices. CdSe NPLs were deposited on NP lattices with narrow SLRs (<4 nm), resulting in the formation of

Received: June 27, 2021
Revised: August 15, 2021
Published: September 2, 2021

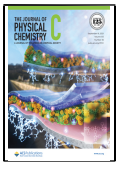

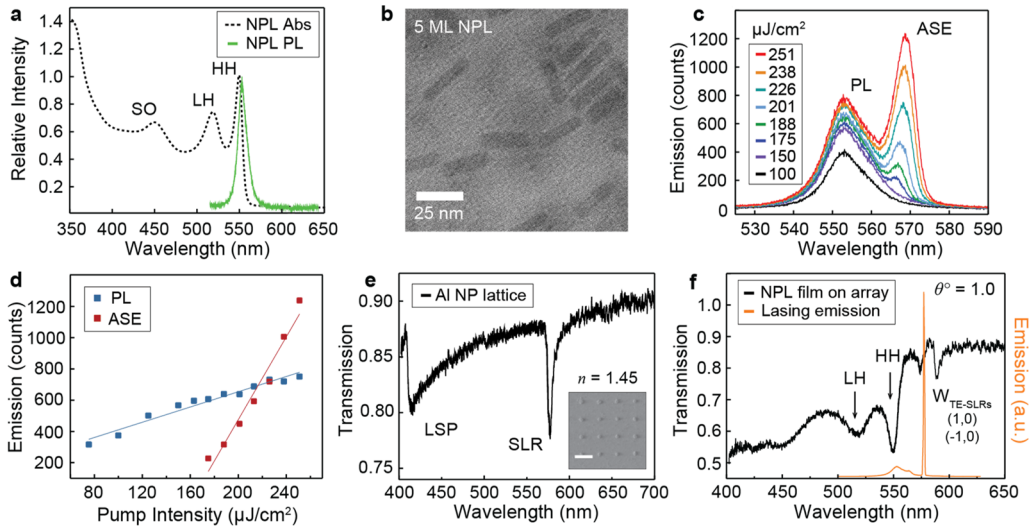

Figure 1. Characterization of 5-monolayer CdSe NPLs on quartz and on a patterned Al NP lattice. (a) UV−vis absorption (dashed line) and photoluminescence (solid line) spectra of 5-monolayer-thick CdSe NPLs. Absorption was measured in hexane solution, and the emission was measured from a drop-cast film. (b) Bright-field transmission electron microscopy image of synthesized NPLs; short edge length = 7.6 ± 0.9 nm and long edge = 24.7 ± 3.0 nm. (c) Emission from CdSe NPLs drop-cast on a quartz substrate as a function of pump fluence with an ASE threshold of 175 $\mu J/cm^2$. (d) Emission intensity at 552 nm shows a sublinear dependence on pump intensity (log−log slope of 0.72 ± 0.003) while the ASE maxima rises superlinearly (4.78 ± 0.11). (e) Transmission spectrum of an Al NP lattice on quartz substrate (n = 1.46 at 570 nm) surrounded by an index-matched oil. Inset: SEM image of a square Al NP lattice. Scale bar is 400 nm. (f) Transmission spectrum of an Al NP lattice with a 150 nm thick CdSe NPL film shows light hole (LH) and heavy hole (HH) absorption features as dips at 512 and 550 nm, respectively; $W_{TE\text{-}SLR}$ modes appear near 574 and 589 nm. Optical excitation above threshold yields narrow spectrum laser emission that overlaps with a W_{TE}-SLR mode.

waveguide SLRs. When optically pumped, nonlinear lasing emission from the hybrid mode was dependent on the NPL film thickness. For NPL films at least 150 nm thick, lasing emission in the far field exhibited small divergence (<1°), low threshold (~200 $\mu J/cm^2$), and ultrafast decay dynamics near the position of the waveguide SLR. Thinner films exhibited only photoluminescence, while thicker films produced waveguided ASE in addition to the surface normal lasing.

RESULTS AND DISCUSSION

CdSe NPLs with a thickness of 5 monolayers were synthesized by using an established protocol[15] and showed narrow band-edge transitions (~12 nm full width at half-maximum (FWHM), Figure 1a and Figure S1). The flat NPL morphology was confirmed by transmission electron microscopy (Figure 1b); the short and long edge dimensions were measured to be 7.6 ± 0.9 nm and 24.7 ± 3.0 nm, respectively. This thickness of the CdSe NPL was selected because of its high synthetic reproducibility and slow Auger recombination relative to thinner 3- and 4-monolayer thick NPLs.[14,15] The refractive index of close-packed CdSe NPLs was determined to be n = 1.8 at 570 nm based on the volume fraction of CdSe (n = 2.56) and oleic acid ligands (n = 1.46).[52] NPLs drop-cast on quartz substrates from a concentrated (~200 mg/mL) dispersion by using a 9:1 hexane:octane solution produced t ~ 150 nm thick films. When pumped at 400 nm with 35 fs pulses, the band-edge PL from single-exciton recombination was observed at low pump intensity (<150 $\mu J/cm^2$). Increasing the pump intensity to 170 $\mu J/cm^2$ produced spectrally narrowed (~7 nm FWHM) amplified spontaneous emission (ASE) near 568 nm in the direction parallel to the plane of the film, with a superlinear intensity dependence on pump fluence that was distinct from the sublinear band-edge emission. The ASE from CdSe NPLs red-shifted to longer wavelengths (566−568 nm) relative to band-edge emission (552 nm) because of attractive biexciton Coulombic interactions and reduced losses from reabsorption (Figures 1c,d).

The large refractive index mismatch of the CdSe NPL film layer (n = 1.8) and the quartz substrate (n = 1.45) results in an optical waveguide upon light excitation.[53] Hybridization between this waveguide mode and the SLR mode from the Al NP lattice produces waveguide surface lattice resonances (W-SLRs).[24,25] Finite-difference time-domain simulations were used to model the properties of the NPL-NP lattice under s-polarized white light with adjustable particle sizes, periodicity, and refractive index environment (Supporting Information). A calculated W-SLR that spectrally overlaps with the NPL gain was supported by Al NPs with diameter d = 75 nm, height h = 60 nm, and lattice periodicity a_0 = 400 nm on a quartz (n = 1.45) substrate (Figure S2). Aluminum was selected as the plasmonic material of interest because of its low losses at both the emission wavelength and the 400 nm optical pump wavelength (Figure S3).[44]

Because previous reports showed that the sidebands of W-SLR modes from colloidal quantum dots at nonzero $k_{||}$ provided optical feedback for lasing,[24,25] we simulated off-normal transmission spectra to identify the W-SLR sidebands from the NPL-NP lattice (Figure S2a). Tuning the angle of incident light between 0° and 1° produced features that correspond to (1,0) and (−1,0) waveguided transverse electric SLR (W_{TE}-SLR) modes; the (1,0) mode is the sideband lasing mode. The experimentally measured lasing emission at 577 nm approximately matches the spectral position of the W_{TE}-SLR sideband mode (587 nm) in the simulated results.

Large-area (cm^2) Al NP lattices were produced using a series of nanofabrication processes described previously (Figure S4).[54] Normal-incidence transmission spectra of the fabricated NP lattice in an index-matched environment of n = 1.45 revealed a spectrally narrow SLR with a 4 nm FWHM at 577 nm (Figure 1e). Transmission spectra of a 150 nm thick NPL

https://doi.org/10.1021/acs.jpcc.1c05662
J. Phys. Chem. C 2021, 125, 19874−19879

film on the same Al NP lattice showed reduced intensity from CdSe NPL absorption features and two W_{TE}-SLR modes with order (1, 0) and (−1,0) (Figure 1f). Figure 2 depicts the

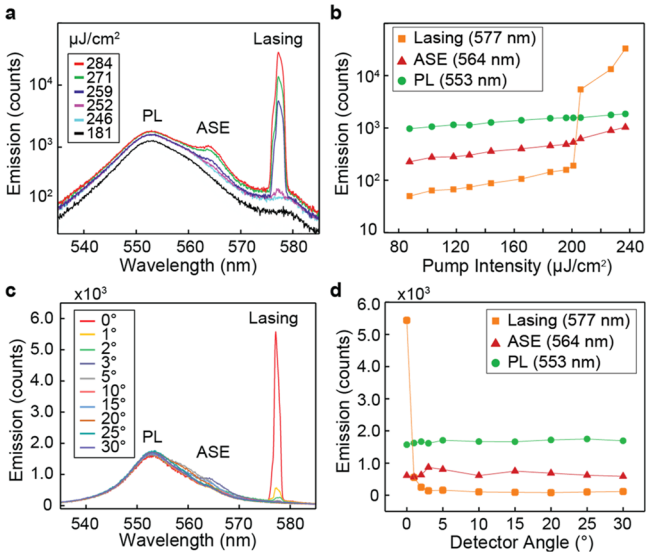

Figure 2. Light emission from a 150 nm thick CdSe NPL film on an Al NP lattice. (a) Normal incidence emission spectra measured for the indicated pump laser fluences show development of strong, spectrally narrow (1 nm FWHM) lasing emission at 577 nm and suppressed ASE at 563 nm. (b) Light emission from different optical processes shows that laser emission grows nonlinearly compared to PL above ~200 $\mu J/cm^2$. (c, d) Emission spectra at different detection angles using a pump fluence of 260 $\mu J/cm^2$ shows highly directional emission for signals near 577 nm in contrast to PL and ASE.

fluence and angle dependence of light emission from the NPL-NP lattices. Emission was collected by using a fiber optic mounted on a concentric rotational stage that directed the light into a spectrograph and CCD. Detecting at normal incidence to the lattice, we measured NPL photoluminescence (PL) at low fluences centered around 553 nm, and then narrowband lasing emission at 577 nm was observed for a fluence of 200 $\mu J/cm^2$ (Figure 2a); this threshold is relatively low compared to that from colloidal quantum dot systems.[24] Emission intensity vs pump fluence shows that the PL follows a linear trend while the 577 nm peak attributed to lasing rises superlinearly and narrows (Figure 2b). Time-correlated single photon counting (TCSPC) and streak camera measurements were used to compare the emission time scales of single-exciton radiative recombination (nanoseconds) with the ultrafast dynamics (picoseconds) of lasing emission (Figure S5).[50] Emission directionality was evaluated by collecting spectra above the lasing threshold as a function of detection angle. The surface normal direction had a divergence of less than 1°, while both PL and ASE showed diffuse scattering (Figures 2c,d).

An important parameter identified to control the emission characteristics of CdSe NPL-Al NP lattices was the thickness of the CdSe NPL film. Drop-cast films produce a "coffee ring effect" where the film is thickest near the droplet edge from particle transport during drying.[55,56] Figure 3a shows an optical micrograph of different NPL film thicknesses on a Al NP lattice. Atomic force microscopy images confirmed that the thickest region of the NPL film was t_2 = 200 nm; the center of the NP lattice and the thinnest film regions were measured to be 150 and 110 nm, respectively (Figures S6 and S7). The average roughness of the NPL film was determined to be 1.96 nm across a 7 μm region as calculated by the root-mean-square method (Figure S8). These different film thicknesses showed distinct behavior when optically pumped. Neither ASE nor lasing was observed for the thinnest (t_1 = 110 nm) NPL region even for the highest pump fluence tested of 356 $\mu J/cm^2$ (Figure 3b). In contrast, for t_2 = 200 nm areas, both ASE and lasing were present (Figure 3c). Note that the intermediate thickness of t = 150 nm in Figure 2a produced lasing with ASE suppressed. Angle-resolved emission showed that lasing signals were emitted normal to the surface (Figure S9), while ASE was observed over a wide range of angles (0°−30°) consistent with incoherent scattering. For thin films, the CdSe NPL layer does not provide enough optical gain to overcome losses of the NP lattice cavity. To determine the minimum NPL film thickness required to observe lasing and ASE, we drop-cast a film using a dilute (20 mg/mL) NPL dispersion (Figure S10). In this case, no ASE was generated, and only PL signals were detected despite exploring high excitation fluences (>1 mJ/cm^2). These three classes of emission depend on the overall thickness of the CdSe NPL film because the refractive index of the film governs the W_{TE}-SLR wavelengths.[24] With an optimal film thickness of 150 nm, the $W_{TE\text{-}SLR}$ cavity mode spectrally overlaps with the NPL emission and shows low-threshold lasing.

CONCLUSIONS

CdSe NPLs can function as high-performance solid-state laser gain media and exhibit room-temperature lasing when integrated with NP lattice nanocavities. Our findings provide

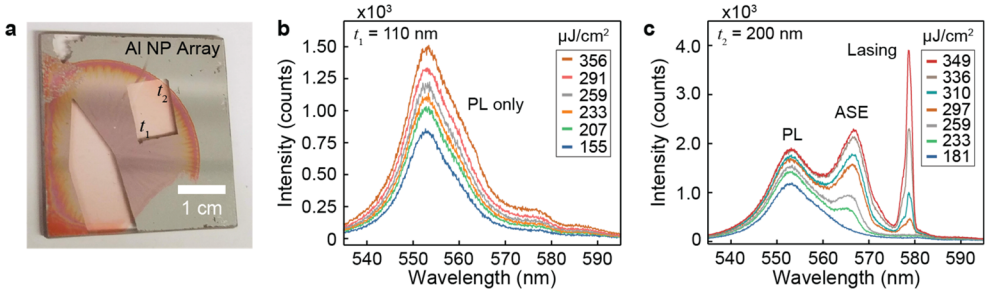

Figure 3. Light emission characteristics for different CdSe NPL film thickness on an Al NP lattice. (a) Optical micrograph of a drop-cast CdSe NPL film on an Al NP lattice. t_1 and t_2 denote regions with thicknesses of 110 and 200 nm, respectively. (b) Emission from the t_1 (thin) region of CdSe NPL film shows neither ASE nor lasing even at high pump fluences. (c) Emission from the t_2 (thick) CdSe NPL film shows both ASE and lasing.

https://doi.org/10.1021/acs.jpcc.1c05662
J. Phys. Chem. C 2021, 125, 19874−19879

insight into how high-index colloidal semiconductor gain can introduce waveguide effects that hybridize with plasmonic lattices. Because NPLs are anisotropic structures, the prospects of controlling particle orientation and thus dipole direction could potentially enable tailoring of the far-field laser beam profile, polarization state, and threshold. We demonstrated the capability of using core-only CdSe NPLs as a gain medium for lasing despite losses from nonradiative Auger recombination. For enhancing lasing performance further, core−shell and gradient shell approaches to growing NPL heterostructures will be investigated to prolong multiexciton lifetimes for increased optical gain.

■ ASSOCIATED CONTENT

Supporting Information

The Supporting Information is available free of charge at https://pubs.acs.org/doi/10.1021/acs.jpcc.1c05662.

Materials and methods used to synthesize CdSe NPLs and additional details on fabrication of Al nanoparticle lattices, measured transmission from neat CdSe NPL film, FDTD simulated transmission spectra, FDTD simulated electric near-field intensity of Al NP lattice, scanning electron microscopy images of lattice fabrication steps, atomic force microscopy characterization of Al NP height, NPL film thickness, and average film roughness, angle-resolved measurement of amplified spontaneous emission (ASE), emission dynamics captured with streak camera, and time-correlated single photon counting (PDF)

■ AUTHOR INFORMATION

Corresponding Author

Teri W. Odom − *Department of Chemistry and Department of Materials Science and Engineering, Northwestern University, Evanston, Illinois 60208, United States;* orcid.org/0000-0002-8490-292X; Email: todom@northwestern.edu

Authors

Nicolas E. Watkins − *Department of Chemistry, Northwestern University, Evanston, Illinois 60208, United States*

Jun Guan − *Department of Chemistry, Northwestern University, Evanston, Illinois 60208, United States;* orcid.org/0000-0001-8667-1611

Benjamin T. Diroll − *Center for Nanoscale Materials, Argonne National Laboratory, Lemont, Illinois 60439, United States;* orcid.org/0000-0003-3488-0213

Kali R. Williams − *Department of Chemistry, Northwestern University, Evanston, Illinois 60208, United States*

Richard D. Schaller − *Department of Chemistry, Northwestern University, Evanston, Illinois 60208, United States; Center for Nanoscale Materials, Argonne National Laboratory, Lemont, Illinois 60439, United States;* orcid.org/0000-0001-9696-8830

Complete contact information is available at: https://pubs.acs.org/10.1021/acs.jpcc.1c05662

Notes

The authors declare no competing financial interest.

■ ACKNOWLEDGMENTS

This work was supported by the National Science Foundation (NSF) under DMR-1904385 (N.E.W., J.G., T.W.O.) and DMREF-16293823 (N.E.W., R.D.S.). This work was supported by the National Science Foundation Graduate Research Fellowship Program under Grant DGE-1324585 (N.E.W.). This work utilized Northwestern University Micro/Nano Fabrication Facility (NUFAB), which is partially supported by Soft and Hybrid Nanotechnology Experimental (SHyNE, NSF ECCS-2025633), the IIN, and Northwestern's MRSEC program (NSF DMR-1720139). This work made use of the EPIC, Keck-II, and/or SPID facilities of Northwestern University's NUANCE Center, which has received support from SHyNE (NSF ECCS-2025633) and the MRSEC program (NSF DMR-1720139). Use of the Center for Nanoscale Materials, an Office of Science user facility, was supported by the U.S. Department of Energy, Office of Science, Office of Basic Energy Sciences, under Contract DE-AC02-06CH11357. This research was supported in part through the computational resources and staff contributions provided by the Quest high performance computing cluster at Northwestern University which is jointly supported by the Office of the Provost, the Office for Research, and Northwestern University Information Technology.

■ REFERENCES

(1) Ithurria, S.; Dubertret, B. Quasi 2D Colloidal CdSe Platelets with Thicknesses Controlled at the Atomic Level. *J. Am. Chem. Soc.* **2008**, *130* (49), 16504−16505.

(2) Ithurria, S.; Tessier, M. D.; Mahler, B.; Lobo, R. P. S. M.; Dubertret, B.; Efros, A. L. Colloidal nanoplatelets with two-dimensional electronic structure. *Nat. Mater.* **2011**, *10* (12), 936−941.

(3) Guzelturk, B.; Kelestemur, Y.; Olutas, M.; Delikanli, S.; Demir, H. V. Amplified spontaneous emission and lasing in colloidal nanoplatelets. *ACS Nano* **2014**, *8* (7), 6599−6605.

(4) She, C.; Fedin, I.; Dolzhnikov, D. S.; Demortière, A.; Schaller, R. D.; Pelton, M.; Talapin, D. V. Low-Threshold Stimulated Emission Using Colloidal Quantum Wells. *Nano Lett.* **2014**, *14* (5), 2772−2777.

(5) Li, Q.; Xu, Z.; McBride, J. R.; Lian, T. Low Threshold Multiexciton Optical Gain in Colloidal CdSe/CdTe Core/Crown Type-II Nanoplatelet Heterostructures. *ACS Nano* **2017**, *11* (3), 2545−2553.

(6) Yang, Z.; Pelton, M.; Fedin, I.; Talapin, D. V.; Waks, E. A room temperature continuous-wave nanolaser using colloidal quantum wells. *Nat. Commun.* **2017**, *8* (1), 143−143.

(7) Guzelturk, B.; Pelton, M.; Olutas, M.; Demir, H. V. Giant Modal Gain Coefficients in Colloidal II−VI Nanoplatelets. *Nano Lett.* **2019**, *19* (1), 277−282.

(8) Van der Bok, J. C.; Dekker, D. M.; Peerlings, M. L. J.; Salzmann, B. B. V.; Meijerink, A. Luminescence Line Broadening of CdSe Nanoplatelets and Quantum Dots for Application in w-LEDs. *J. Phys. Chem. C* **2020**, *124* (22), 12153−12160.

(9) Klimov, V. I.; Mikhailovsky, A. A.; Xu, S.; Malko, A.; Hollingsworth, J. A.; Leatherdale, C. A.; Eisler, H. J.; Bawendi, M. G. Optical Gain and Stimulated Emission in Nanocrystal Quantum Dots. *Science* **2000**, *290* (5490), 314.

(10) Kazes, M.; Lewis, D. Y.; Ebenstein, Y.; Mokari, T.; Banin, U. Lasing from Semiconductor Quantum Rods in a Cylindrical Microcavity. *Adv. Mater.* **2002**, *14* (4), 317−321.

(11) Chen, Z.; Nadal, B.; Mahler, B.; Aubin, H.; Dubertret, B. Quasi-2D Colloidal Semiconductor Nanoplatelets for Narrow Electroluminescence. *Adv. Funct. Mater.* **2014**, *24* (3), 295−302.

(12) Baghani, E.; O'Leary, S. K.; Fedin, I.; Talapin, D. V.; Pelton, M. Auger-Limited Carrier Recombination and Relaxation in CdSe

Colloidal Quantum Wells. *J. Phys. Chem. Lett.* **2015**, *6* (6), 1032−1036.
(13) Fan, F.; Voznyy, O.; Sabatini, R. P.; Bicanic, K. T.; Adachi, M. M.; McBride, J. R.; Reid, K. R.; Park, Y.-S.; Li, X.; Sargent, E. H.; et al. Continuous-wave lasing in colloidal quantum dot solids enabled by facet-selective epitaxy. *Nature* **2017**, *544* (7648), 75−79.
(14) Li, Q.; Lian, T. Area- and Thickness-Dependent Biexciton Auger Recombination in Colloidal CdSe Nanoplatelets: Breaking the "Universal Volume Scaling Law. *Nano Lett.* **2017**, *17* (5), 3152−3158.
(15) She, C.; Fedin, I.; Dolzhnikov, D. S.; Dahlberg, P. D.; Engel, G. S.; Schaller, R. D.; Talapin, D. V. Red, Yellow, Green, and Blue Amplified Spontaneous Emission and Lasing Using Colloidal CdSe Nanoplatelets. *ACS Nano* **2015**, *9* (10), 9475−9485.
(16) Kunneman, L. T.; Tessier, M. D.; Heuclin, H.; Dubertret, B.; Aulin, Y. V.; Grozema, F. C.; Schins, J. M.; Siebbeles, L. D. Bimolecular Auger recombination of electron−hole pairs in two-dimensional CdSe and CdSe/CdZnS core/shell nanoplatelets. *J. Phys. Chem. Lett.* **2013**, *4* (21), 3574−3578.
(17) Siegman, A. E. *Lasers*. University Science Books; Revised ed., **1986**.
(18) Malko, A.; Mikhailovsky, A.; Petruska, M.; Hollingsworth, J.; Htoon, H.; Bawendi, M.; Klimov, V. I. From amplified spontaneous emission to microring lasing using nanocrystal quantum dot solids. *Appl. Phys. Lett.* **2002**, *81* (7), 1303−1305.
(19) Snee, P. T.; Chan, Y.; Nocera, D. G.; Bawendi, M. G. Whispering-gallery-mode lasing from a semiconductor nanocrystal/microsphere resonator composite. *Adv. Mater.* **2005**, *17* (9), 1131−1136.
(20) Eisler, H.-J.; Sundar, V. C.; Bawendi, M. G.; Walsh, M.; Smith, H. I.; Klimov, V. Color-selective semiconductor nanocrystal laser. *Appl. Phys. Lett.* **2002**, *80* (24), 4614−4616.
(21) Kozlov, O. V.; Park, Y.-S.; Roh, J.; Fedin, I.; Nakotte, T.; Klimov, V. I. Sub−single-exciton lasing using charged quantum dots coupled to a distributed feedback cavity. *Science* **2019**, *365* (6454), 672−675.
(22) Dang, C.; Lee, J.; Breen, C.; Steckel, J. S.; Coe-Sullivan, S.; Nurmikko, A. Red, green and blue lasing enabled by single-exciton gain in colloidal quantum dot films. *Nat. Nanotechnol.* **2012**, *7* (5), 335−339.
(23) Altug, H.; Englund, D.; Vučković, J. Ultrafast photonic crystal nanocavity laser. *Nat. Phys.* **2006**, *2*, 484−484.
(24) Guan, J.; Sagar, L. K.; Li, R.; Wang, D.; Bappi, G.; Wang, W.; Watkins, N.; Bourgeois, M. R.; Levina, L.; Odom, T. W.; et al. Quantum Dot-Plasmon Lasing with Controlled Polarization Patterns. *ACS Nano* **2020**, *14* (3), 3426−3433.
(25) Guan, J.; Sagar, L. K.; Li, R.; Wang, D.; Bappi, G.; Watkins, N. E.; Bourgeois, M. R.; Levina, L.; Fan, F.; Odom, T. W.; et al. Engineering Directionality in Quantum Dot Shell Lasing Using Plasmonic Lattices. *Nano Lett.* **2020**, *20* (2), 1468−1474.
(26) Fernandez-Bravo, A.; Wang, D.; Barnard, E. S.; Teitelboim, A.; Tajon, C.; Guan, J.; Schatz, G. C.; Cohen, B. E.; Chan, E. M.; Odom, T. W.; et al. Ultralow-threshold, continuous-wave upconverting lasing from subwavelength plasmons. *Nat. Mater.* **2019**, *18* (11), 1172−1176.
(27) Wang, D.; Wang, W.; Knudson, M. P.; Schatz, G. C.; Odom, T. W. Structural Engineering in Plasmon Nanolasers. *Chem. Rev.* **2018**, *118* (6), 2865−2881.
(28) Wang, D.; Bourgeois, M. R.; Guan, J.; Fumani, A. K.; Schatz, G. C.; Odom, T. W. Lasing from Finite Plasmonic Nanoparticle Lattices. *ACS Photonics* **2020**, *7* (3), 630−636.
(29) Zhou, W.; Dridi, M.; Suh, J. Y.; Kim, C. H.; Co, D. T.; Wasielewski, M. R.; Schatz, G. C.; Odom, T. W. Lasing action in strongly coupled plasmonic nanocavity arrays. *Nat. Nanotechnol.* **2013**, *8* (7), 506−511.
(30) Wang, D.; Bourgeois, M. R.; Lee, W.-K.; Li, R.; Trivedi, D.; Knudson, M. P.; Wang, W.; Schatz, G. C.; Odom, T. W. Stretchable Nanolasing from Hybrid Quadrupole Plasmons. *Nano Lett.* **2018**, *18* (7), 4549−4555.
(31) Wang, D.; Yang, A.; Wang, W.; Hua, Y.; Schaller, R. D.; Schatz, G. C.; Odom, T. W. Band-edge engineering for controlled multi-modal nanolasing in plasmonic superlattices. *Nat. Nanotechnol.* **2017**, *12* (9), 889−894.
(32) Guan, J.; Bourgeois, M. R.; Li, R.; Hu, J.; Schaller, R. D.; Schatz, G. C.; Odom, T. W. Identification of Brillouin Zones by In-Plane Lasing from Light-Cone Surface Lattice Resonances. *ACS Nano* **2021**, *15* (3), 5567−5573.
(33) Knudson, M. P.; Li, R.; Wang, D.; Wang, W.; Schaller, R. D.; Odom, T. W. Polarization-Dependent Lasing Behavior from Low-Symmetry Nanocavity Arrays. *ACS Nano* **2019**, *13* (7), 7435−7441.
(34) Lin, Y.; Wang, D.; Hu, J.; Liu, J.; Wang, W.; Guan, J.; Schaller, R. D.; Odom, T. W. Engineering Symmetry-Breaking Nanocrescent Arrays for Nanolasing. *Adv. Funct. Mater.* **2019**, *29* (42), 1904157.
(35) Cherqui, C.; Bourgeois, M. R.; Wang, D.; Schatz, G. C. Plasmonic Surface Lattice Resonances: Theory and Computation. *Acc. Chem. Res.* **2019**, *52* (9), 2548−2558.
(36) Wang, W.; Ramezani, M.; Väkeväinen, A. I.; Törmä, P.; Rivas, J. G.; Odom, T. W. The rich photonic world of plasmonic nanoparticle arrays. *Mater. Today* **2018**, *21* (3), 303−314.
(37) Kravets, V. G.; Kabashin, A. V.; Barnes, W. L.; Grigorenko, A. N. Plasmonic Surface Lattice Resonances: A Review of Properties and Applications. *Chem. Rev.* **2018**, *118* (12), 5912−5951.
(38) Auguié, B.; Barnes, W. L. Collective Resonances in Gold Nanoparticle Arrays. *Phys. Rev. Lett.* **2008**, *101* (14), 143902.
(39) Li, R.; Bourgeois, M. R.; Cherqui, C.; Guan, J.; Wang, D.; Hu, J.; Schaller, R. D.; Schatz, G. C.; Odom, T. W. Hierarchical Hybridization in Plasmonic Honeycomb Lattices. *Nano Lett.* **2019**, *19* (9), 6435−6441.
(40) Wang, D.; Yang, A.; Hryn, A. J.; Schatz, G. C.; Odom, T. W. Superlattice Plasmons in Hierarchical Au Nanoparticle Arrays. *ACS Photonics* **2015**, *2* (12), 1789−1794.
(41) Zou, S.; Janel, N.; Schatz, G. C. Silver nanoparticle array structures that produce remarkably narrow plasmon lineshapes. *J. Chem. Phys.* **2004**, *120* (23), 10871−10875.
(42) Yang, A.; Hryn, A. J.; Bourgeois, M. R.; Lee, W.-K.; Hu, J.; Schatz, G. C.; Odom, T. W. Programmable and reversible plasmon mode engineering. *Proc. Natl. Acad. Sci. U. S. A.* **2016**, *113* (50), 14201.
(43) Deng, S.; Li, R.; Park, J.-E.; Guan, J.; Choo, P.; Hu, J.; Smeets, P. J. M.; Odom, T. W. Ultranarrow plasmon resonances from annealed nanoparticle lattices. *Proc. Natl. Acad. Sci. U. S. A.* **2020**, *117* (38), 23380.
(44) Li, R.; Wang, D.; Guan, J.; Wang, W.; Ao, X.; Schatz, G. C.; Schaller, R.; Odom, T. W. Plasmon nanolasing with aluminum nanoparticle arrays. *J. Opt. Soc. Am. B* **2019**, *36* (7), E104−E111.
(45) Pourjamal, S.; Hakala, T. K.; Nečada, M.; Freire-Fernández, F.; Kataja, M.; Rekola, H.; Martikainen, J.-P.; Törmä, P.; van Dijken, S. Lasing in Ni Nanodisk Arrays. *ACS Nano* **2019**, *13* (5), 5686−5692.
(46) Deng, S.; Zhang, B.; Choo, P.; Smeets, P. J. M.; Odom, T. W. Plasmonic Photoelectrocatalysis in Copper−Platinum Core−Shell Nanoparticle Lattices. *Nano Lett.* **2021**, *21* (3), 1523−1529.
(47) Reese, T.; Reed, A. N.; Sample, A. D.; Freire-Fernández, F.; Schaller, R. D.; Urbas, A. M.; Odom, T. W. Ultrafast Spectroscopy of Plasmonic Titanium Nitride Nanoparticle Lattices. *ACS Photonics* **2021**, *8* (6), 1556−1561.
(48) Wang, D.; Guan, J.; Hu, J.; Bourgeois, M. R.; Odom, T. W. Manipulating Light−Matter Interactions in Plasmonic Nanoparticle Lattices. *Acc. Chem. Res.* **2019**, *52* (11), 2997−3007.
(49) Guo, R.; Nečada, M.; Hakala, T. K.; Väkeväinen, A. I.; Törmä, P. Lasing at K Points of a Honeycomb Plasmonic Lattice. *Phys. Rev. Lett.* **2019**, *122* (1), 013901.
(50) Wang, W.; Watkins, N.; Yang, A.; Schaller, R. D.; Schatz, G. C.; Odom, T. W. Ultrafast Dynamics of Lattice Plasmon Lasers. *J. Phys. Chem. Lett.* **2019**, *10* (12), 3301−3306.
(51) Daskalakis, K. S.; Väkeväinen, A. I.; Martikainen, J.-P.; Hakala, T. K.; Törmä, P. Ultrafast Pulse Generation in an Organic Nanoparticle-Array Laser. *Nano Lett.* **2018**, *18* (4), 2658−2665.

https://doi.org/10.1021/acs.jpcc.1c05662
J. Phys. Chem. C 2021, 125, 19874−19879

(52) Zhang, Z.; Thung, Y. T.; Chen, X.; Wang, L.; Fan, W.; Ding, L.; Sun, H. Study of Complex Optical Constants of Neat Cadmium Selenide Nanoplatelets Thin Films by Spectroscopic Ellipsometry. *J. Phys. Chem. Lett.* **2021**, *12* (1), 191−198.
(53) Adams, M. J. *An Introduction to Optical Waveguides*; John Wiley & Sons: 1981.
(54) Lee, M. H.; Huntington, M. D.; Zhou, W.; Yang, J.-C.; Odom, T. W. Programmable Soft Lithography: Solvent-Assisted Nanoscale Embossing. *Nano Lett.* **2011**, *11* (2), 311−315.
(55) Anyfantakis, M.; Baigl, D. Manipulating the Coffee-Ring Effect: Interactions at Work. *ChemPhysChem* **2015**, *16* (13), 2726−2734.
(56) Kaplan, C. N.; Mahadevan, L. Evaporation-driven ring and film deposition from colloidal droplets. *J. Fluid Mech.* **2015**, *781*, R2.

https://doi.org/10.1021/acs.jpcc.1c05662
J. Phys. Chem. C 2021, 125, 19874−19879